

PACS numbers: 42.65.Hw; 42.65.Jx; 42.65.Wi
DOI: 10.1070/QE2011v041n11ABEH014625

Filamentation of femtosecond laser radiation with a non-Gaussian transverse spatial profile

A.A. Biryukov, N.A. Panov, M.V. Volkov, D.S. Uryupina, R.V. Volkov, O.G. Kosareva, A.B. Savel'ev

Abstract. **The filamentation of a femtosecond laser pulse with a non-Gaussian transverse intensity profile has been studied experimentally and by numerical simulation. The results demonstrate that the distance to the filamentation region can be evaluated using the Marburger formula in which the critical power of self-focusing at a beam quality factor M^2 exceeds that for a Gaussian beam by a factor of $(M^2)^2$. The characteristics of the filament resulting from self-focusing depend little on the beam quality factor: both the filament energy and diameter coincide. If the beam is passed through an aperture, a filament forms on a diffraction ring, and its parameters coincide with those of a filament formed with no slit (provided the initial pulse parameters coincide).**

Keywords: *femtosecond laser pulse, filamentation, critical power for self-focusing, multimode radiation.*

1. Introduction

The formation of extended channels of nanosecond laser radiation due to self-focusing in air was demonstrated experimentally by Basov et al. [1] in the late 1960s, and the filamentation of high-power femtosecond laser pulses in gases at atmospheric pressure was first reported in the mid-1990s [2]. The filamentation of laser radiation has since been the subject of intense research [3, 4]. This phenomenon is of interest in relation to remote sensing [5], generation of high-power few-cycle optical pulses [6], terahertz radiation generation [7, 8], third-harmonic generation [9, 10], polarisation ellipse rotation at the fundamental [11, 12] and second-harmonic [13, 14] frequencies, four-wave mixing in filaments [15] and other issues and effects.

Most filamentation-related nonlinear optical phenomena were studied experimentally using a focused beam [3, 4] generating a single filament. For a number of applications, however, a collimated geometry was shown to be more advantageous [16–18]. The peak pulse power in Refs [16–18] exceeded the critical power only slightly, so no multiple filamentation developed. In theoretical and numerical studies of filamentation-induced nonlinear processes, the beam incident on a nonlinear medium is usually taken to be axisymmetric [3, 4]. At the same time, amplitude and phase distortions of the transverse intensity profile in real laser systems accumulate in the amplifier cascade, and the output beam profile turns out to be amplitude- and phase-modulated, i.e. the beam becomes multimode. This is of particular importance for high-power laser systems with a 10-Hz pulse repetition rate because they have a considerable number of amplifiers and are subject to transient thermal lensing (the beam quality factor of such systems without adaptive mirrors is typically well above unity).

In this paper, we present an experimental study and numerical simulation of the formation and evolution of a filament produced by the beam of a Ti:sapphire laser system pulsed at a repetition rate of 10 Hz.

A.A. Biryukov, N.A. Panov, M.V. Volkov, D.S. Uryupina, R.V. Volkov, O.G. Kosareva, A.B. Savel'ev International Laser Center, M.V. Lomonosov Moscow State University, Vorob'evy gory 1, 119991 Moscow, Russia; e-mail: napanov@ilc.edu.ru

Received 6 April 2011; revision received 8 June 2011
Kvantovaya Elektronika **41** (11) 958–962 (2011)
Translated by O.M. Tsarev

2. Filamentation of a multimode beam: experiment and computer simulation

In our experiments (Fig. 1), 55-fs pulses of 805-nm radiation (pulse energy in the range 0.5–2.5 mJ, repetition rate of 10 Hz) travelled a distance $l = 6$ m from the output of the compressor of the laser system [19] to a telescope (the slit shown in Fig. 1 was not used). The average full width at half maximum (FWHM) diameter of the multimode beam ($M^2 \approx 1.4 \pm 0.1$) was 7 mm, and the peak intensity was $I \approx 10^{11}$ W cm^{-2}, so the phase shift due to Kerr nonlinearity, $n_2 Ikl$, over a distance of 6 m was within 0.5 rad ($n_2 = 10^{-19}$ cm^2 W^{-1}; k is the wavenumber corresponding to wavelength λ). Using a telescope consisting of a lens ($F = 4.52$ m) and spherical dielectric mirror ($F = -1$ m), the beam was compressed to an FWHM diameter of 1.5 mm and directed to the required path (the path length was measured from the surface of the spherical mirror of the telescope, $z = 0$) for filament formation.

In the beam path from the spherical mirror, a photodetector system was mounted on a purpose-designed rail. The system comprised a quartz wedge reflecting 4% of incident radiation, calibrated attenuation filters and an Ormins Model U2C-14S415 CCD camera (782 × 582 pixels; pixel size, 8.3 μm). To measure the transverse energy density distribution, the wedge holder, rigidly connected to the CCD camera, was translated along the filament on the rail ($z = 1.3$–4 m). The image from the CCD camera was fed to a computer for analysis and comparison with numerical simulation results. The main characteristic to be measured was the energy density distribution, $F(x, y, z)$, which was found as the time integral of the intensity at a distance z:

$$F(x,y,z) = \int_{-\infty}^{\infty} I(x,y,z,t)\mathrm{d}t. \quad (1)$$

The transverse energy density distribution measured a distance $z = 1.3$ m from the spherical mirror (Fig. 2a) had a characteristic FWHM size of 500 μm (Fig. 2a, black contours).

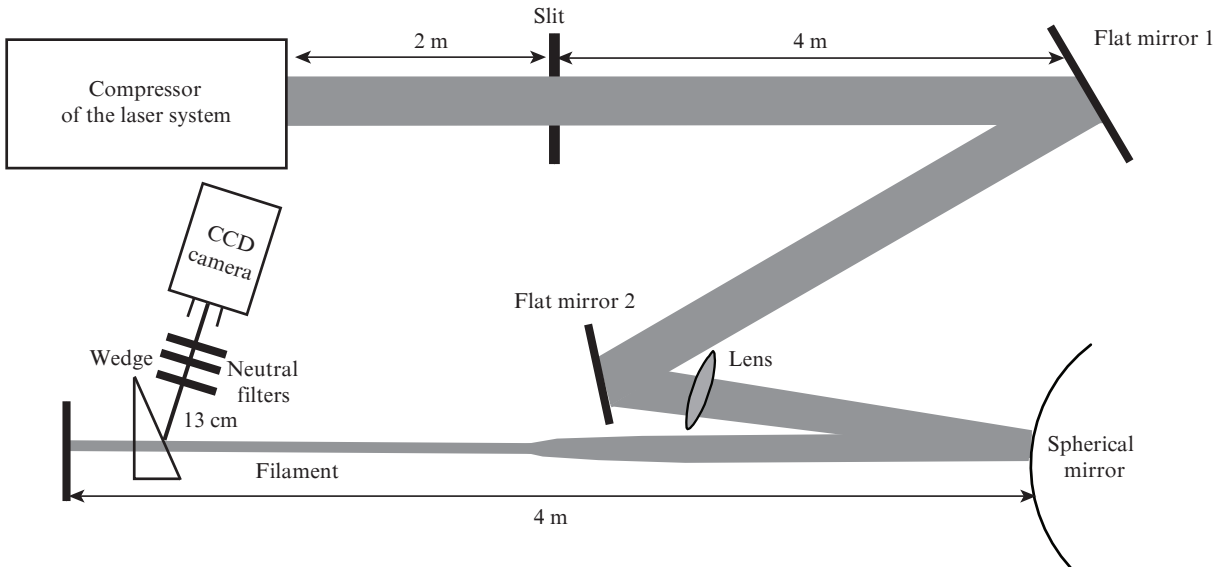

Figure 1. Schematic of the experimental setup for investigation of the filamentation of high-power laser pulses with a multimode beam structure.

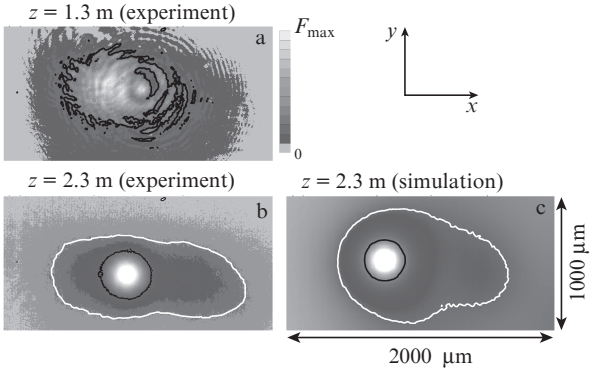

Figure 2. Energy density distributions for pulse filamentation: (a) multimode distribution, (b) distribution containing an axisymmetric mode, (c) simulated distribution. The black contours indicate the half-maximum level of the energy density at a given z value.

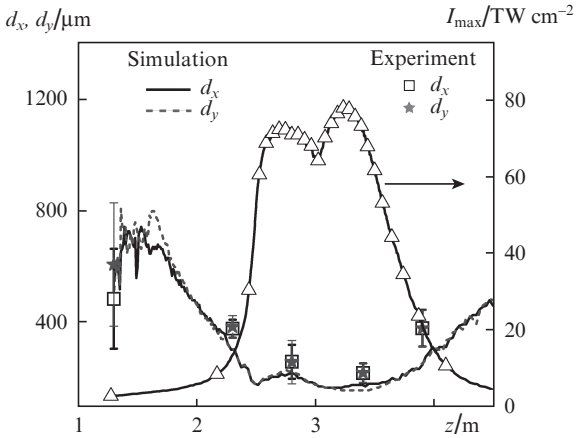

Figure 3. Beam diameter as a function of z (experimental data and numerical simulation in a 3D time-dependent model) and peak intensity as a function of z (simulation results).

In the beam path accessible for measurements, filament formation was observed starting at pulse energies of 1.5 mJ. The front end of the filament corresponded to an axisymmetric mode (Fig. 2b, $z = 2.3$ m), which correlates with evidence for beam profile symmetrisation and 'cleaning' upon femtosecond pulse filamentation in air [20] and water [21]. The axisymmetric profile persisted throughout the filament.

The z-coordinate where filament formation begins can be evaluated as [22]

$$z_f = \frac{0.367ka^2}{\{[(P/P_{crit})^{1/2} - 0.852]^2 - 0.0219\}^{1/2}}, \quad (2)$$

where a is the 1/e beam radius. At a pulse energy of 2.5 mJ, the self-focusing distance, z_f, coincides with the experimentally determined value (Fig. 3, square and asterisk at $z = 2.3$ m) if the critical power for multimode beam self-focusing, P_{crit}, is taken to be 20 GW, i.e. twice the critical power for an axisymmetric Gaussian beam in air ($P_{crit\,G} = 10$ GW [3, 4]). The initial pulse energy of 1.5 mJ is the lowest possible for filamentation under the conditions of our experiments ($P/P_{crit} = 1.3$). Because of the high critical power for self-focusing, no multiple filamentation was observed in our experiments at pulse energies of up to 2.5 mJ.

The beam quality factor, M^2, is the ratio of the divergence of a beam to that of a Gaussian beam, and the critical power for self-focusing of a Gaussian beam is near the lowest level [3, 4]. It is therefore reasonable to expect that the first to focus will be a nearly Gaussian mode, with a critical power $P_{crit\,G}$. The critical power for a multimode beam is then

$$P_{crit} \approx (M^2)^2 P_{crit\,G}. \quad (3)$$

Indeed, according to experimental data we have $M^2 \approx 1.4$, $P_{crit\,G} = 10$ GW. Since we take $P_{crit} \approx 20$ GW in (2), relation (3) is fulfilled.

In numerical simulation of multimode beam filamentation, we used a three-dimensional (3D) time-dependent model for light propagation (in x, y, z, and t coordinates) [23, 24]. The energy density distribution in Fig. 2a, with a flat phase front, was used as the initial condition. The initial pulse energy was $W_0 = 2.5$ mJ, and the pulse FWHM was 55 fs. Figure 2c shows the simulated energy density distribution at a

distance corresponding to filament formation (z = 2.3 m). Like in our experiments, higher order modes are eliminated in the simulation, leading to the formation of an axisymmetric mode as a result of self-focusing [25] in the filament (Figs 2b, 2c, black contours), and the low-energy-density background has a quasi-elliptical distribution, in reasonable agreement with the experimental data (Figs 2b, 2c, white contours).

The formation of an axisymmetric mode in our experiments and numerical simulations is illustrated by the variations of the filament FWHM in two mutually perpendicular directions (d_x and d_y) with z in Fig. 3. In the initial stage of filament formation, at relatively low intensities (z = 1.3–1.7 m), both d_x and d_y vary markedly. For $z > 1.7$ m, they decrease monotonically. After filament formation, at z = 2.3 m, $d_x = d_y = d$ to within ~2%, i.e. the transverse energy density distribution is axisymmetric. The simulated beam size (minimum diameter, 160 μm) agrees with experimental data (200 μm) if the diffraction-induced beam divergence in the measurement system is taken into account. According to Kosareva et al. [26], the calculated peak intensity is limited to 75 TW cm^{-2} by a self-induced laser plasma. In our simulations, the high-intensity region with an axisymmetric spatial profile about 200 μm in diameter extends over about 1.5 m (z = 2.5–4 m). Note that it is in this region where efficient compression of a 50-fs laser pulse to several femtoseconds is possible [6, 16–18].

When a multimode laser beam is used in experiments, the energy of the axisymmetric mode of the filament (Figs 2b, 2c) would be expected to be lower in comparison with an originally Gaussian beam. It is necessary to evaluate the filament energy because the efficiency of nonlinear optical conversion of the input pulse energy may be lower in the case of a multimode beam. In both experiments and numerical simulations, the filament energy, $W_{1/2}$, can be found by integrating over the region of the beam, Σ, where the energy density, $F(x, y, z)$, is at least half the maximum energy density, F_{max}, at the same value of z:

$$W_{1/2}(z) = \iint_{\Sigma} F(x,y,z)\,\mathrm{d}x\mathrm{d}y. \qquad (4)$$

At the beginning of the beam path (z = 0 for a Gaussian beam and z = 1.3 m for a multimode beam), $W_{1/2}$ is ~1 mJ for both an axisymmetric Gaussian beam and a multimode beam (Fig. 4, dashed and solid lines, respectively). Beam self-compression as a result of self-focusing reduces $W_{1/2}$ (the area of integration with respect to transverse coordinates decreases more rapidly in comparison with the increase in energy density in it), which drops to a local minimum at the beginning of the filament: at z = 0.75 m in the case of an ideal Gaussian beam and at z = 2.3 m in the case of a multimode beam (Fig. 4, dashed and solid lines). With increasing distance along the filament, $W_{1/2}$ drops to 80–100 μJ for both a Gaussian and a multimode initial spatial distribution. The compressed pulse duration in the axisymmetric mode of a filament 160–200 μm in diameter (Fig. 3) reaches 7–8 fs [6, 16–18] and is independent of the initial energy density distribution across the beam. Thus, the energy of a pulse compressed to a minimum duration of 7–8 fs is ~100 μJ and depends only slightly on initial beam quality. Note however that the distance where such a pulse forms depends significantly on initial beam quality.

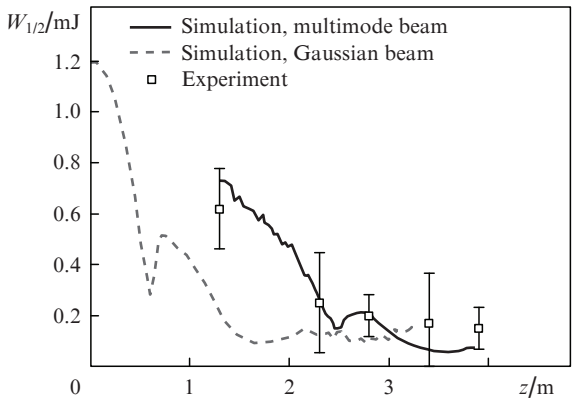

Figure 4. Energy in the highest intensity part of the beam, $W_{1/2}$, as a function of z.

3. Filament formation in an apertured beam

Travelling over a few to tens of metres, a light beam always encounters apertures whose diameter exceeds the beam diameter (mirrors, beam splitters, polarisers, etc.). This changes the convergence and transverse intensity profile of the beam through diffraction effects. In connection with this, we carried out a number of experiments concerned with filament formation when a beam was passed through an 18-mm-diameter aperture mounted 2 m from the compressor (recall that the FWHM beam diameter in our experiments was 7 mm; see Fig. 1). For comparison, an experiment was performed with no slit. The beam parameters in that experiment were the same as in the preceding experiment except that the pulse energy was 4.5 mJ both in the presence of the slit and without it, and the beam quality factor was $M^2 = 1.8 \pm 0.1$.

Filament formation in a beam passed through an aperture (Fig. 5a) differs from that with no slit (Fig. 5b): as a result of the diffraction from the edge of the slit, the beam acquires a ring structure in which the inhomogeneity of the transverse intensity profile above the critical power for self-focusing produces a filament. Filament formation from a ring structure similar to that in Fig. 5a was also demonstrated by numerical simulation [27]. At the same time, when there was no slit, a filament was produced approximately at the beam axis.

When a slit is mounted in the beam path, filamentation develops earlier (see also experimental data and simulation results in Daigle et al. [27]) than with no slit because there is a primary disturbance in the beam and its effective diameter is smaller than the total beam diameter [see Eqn (2)]. This is supported by the data in Fig. 6, which shows the beam diameter, d, as a function of beam path, z, in experiments with a slit (z = 1.5 m; at smaller distances, the beam diameter cannot be evaluated because of the ring structure) and without it. Indeed, the beam diameter drops to ~500 μm at z = 1.5 m after the aperture and at z = 2.4 m when there is no slit. Subsequent evolution of the filament with increasing distance differs little from that with no slit: its parameters stabilise. Note also that, when there is no slit, the filament formation distance is consistent with Eqns (2) and (3) given that both the pulse energy and beam quality factor in this experiment exceed those in the first experiment.

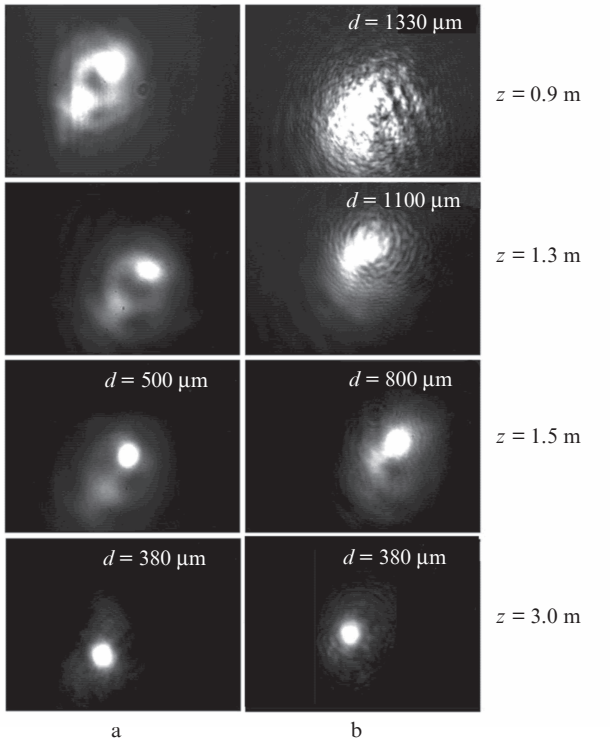

Figure 5. Comparison of filament formation dynamics (a) with a slit and (b) without it.

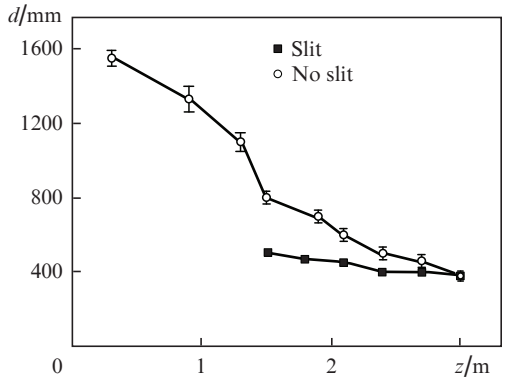

Figure 6. Beam diameter as a function of distance z along the beam path with a slit and without it.

4. Conclusions

Our experiments and numerical simulations demonstrate that the self-focusing distance of high-power multimode femtosecond radiation from a typical Ti:sapphire laser system can be evaluated using the Marburger formula (2), in which the critical power of self-focusing exceeds that for an ideal Gaussian beam by a factor of $(M^2)^2$. The characteristics of the filament resulting from self-focusing depend little on the beam quality factor: both the filament energy and diameter coincide. This means that various nonlinear effects can be detected in a filament formed from a collimated multimode beam, but the distance from the telescope where they can be detected will exceed that in the case of a beam with an initially Gaussian intensity profile.

If the beam is passed (before the telescope) through an aperture whose diameter exceeds the FWHM beam diameter, filament formation occurs on a ring structure that results from diffraction by the edge of the slit. Nevertheless, the distance to the beginning of a quasi-steady-state filament formed under such conditions, its dynamics and its energy are not influenced by the slit.

Acknowledgements. This work was supported in part by the Russian Foundation for Basic Research (Grant Nos 09-02-01200-a and 09-02-01522-a), the RF President's Grants Council (Support to Young Russian Candidates of Science Programme, Grant No. MK-2213.2010.2) and the RF Ministry of Education and Science (State Contract No. 02.740.11.0223).

References

1. Basov N.G., Kryukov P.G., Senatskii Yu.V., Chekalin S.V. *Zh. Eksp. Teor. Fiz.*, **57**, 1175 (1969).
2. Braun A., Korn G., Liu X., Du D., Squier J., Mourou G. *Opt. Lett.*, **20**, 73 (1995).
3. Couairon A., Mysyrowicz A. *Phys. Rep.*, 441, 47 (2007).
4. Kandidov V.P., Shlenov S.A., Kosareva O.G. *Kvantovaya Elektron.*, **39**, 205 (2009) [*Quantum Electron.*, **39**, 205 (2009)].
5. Kasparian J., Rodrigues M., Mejean G., Yu J., Salmon E., Wille H., Bourayou R., Frey S., Andre Y.-B., Mysyrowicz A., Sauerbrey R., Wolf J.-P., Wöste L. *Science*, **301**, 61 (2003).
6. Hauri C.P., Kornelis W., Helbing F.W., Heinrich A., Couairon A., Mysyrowicz A., Biegert J., Keller U. *Appl. Phys. B*, **79**, 673 (2004).
7. Xie X., Dai J., Zhang X.-C. *Phys. Rev. Lett.*, **96**, 075005 (2006).
8. d'Amico C., Houard A., Akturk S., Liu Y., le Bloas J., Franco M., Prade B., Couairon A., Tikhonchuk V.T., Mysyrowicz A. *New J. Phys.*, **10**, 013015 (2008).
9. Akozbek N., Iwasaki A., Becker A., Scalora M., Chin S.L., Bowden C.M. *Phys. Rev. Lett.*, **89**, 143901 (2002).
10. Akozbek N., Trushin S.A., Baltuska A., Fuss W., Goulielmakis E., Kosma K., Krausz F., Panja S., Uiberacker M., Schmid W.E., Becker A., Scalora M., Bloemer M. *New J. Phys.*, **8**, 177 (2006).
11. Kolesik M., Moloney J.V., Wright E.M. *Phys. Rev. E*, **64**, 046607 (2001).
12. Panov N.A., Kosareva O.G., Savel'ev A.B., Uryupina D.S., Perezhogin I.A., Makarov V.A. *Kvantovaya Elektron.*, **41**, 160 (2011) [Quantum Electron., **41**, 160 (2011)].
13. Béjot P., Petit Y., Bonacina L., Kasparian J., Moret M., Wolf J.-P. *Opt. Express*, **16**, 7564 (2008).
14. Kosareva O., Panov N., Makarov V., Perezhogin I., Marceau C., Chen Y., Yuan S., Wang T., Zeng H., Savel'ev A., Chin S.L. *Opt. Lett.*, **35**, 2904 (2010).
15. Theberge F., Akozbek N., Liu W.W., Becker A., Chin S.L. *Phys. Rev. Lett.*, **97**, 023904 (2006).
16. Uryupina D., Kurilova M., Mazhorova A., Panov N., Volkov R., Gorgutsa S., Kosareva O., Savel'ev A., Chin S.L. *J. Opt. Soc. Am. B*, **27**, 667 (2010).
17. Kurilova M.V., Uryupina D.S., Mazhorova A.V., Volkov R.V., Gorgutsa S.R., Panov N.A., Kosareva O.G., Savel'ev A.B. *Kvantovaya Elektron.*, **39**, 879 (2009) [*Quantum Electron.*, **39**, 879 (2009)].
18. Kosareva O.G., Panov N.A., Uryupina D.S., Kurilova M.V., Mazhorova A.V., Savel'ev A.B., Volkov R.V., Kandidov V.P., Chin S.L. *Appl. Phys. B*, **91**, 35 (2008).
19. Bol'shakov V.V., Vorob'ev A.A., Volkov R.V., Knyaz'kov V.A., Eremin N.V., Paskhalov A.A., Shevel'ko A.P., Kazakov E.D., Romanovskii M.Yu., Savel'ev A.B. *Prikl. Fiz.*, **1**, 18 (2009).
20. Prade B., Franco M., Mysyrowicz A., Couairon A., Buersing H., Eberle B., Krenz M., Seiffer D., Vasseur O. *Opt. Lett.*, **31**, 2601 (2006).
21. Liu W., Chin S.L. *Phys. Rev. A*, **76**, 013826 (2007).
22. Marburger J.H. *Prog. Quantum Electron.*, **4**, 35 (1975).

23. Hosseini S.A., Luo Q., Ferland B., Liu W., Chin S.L., Kosareva O.G., Panov N.A., Aközbek N., Kandidov V.P. *Phys. Rev. A*, **70**, 033802 (2004).
24. Panov N.A., Kosareva O.G., Kandidov V.P., Akozbek N., Scalora M., Chin S.L. *Kvantovaya Elektron*., **37**, 1153 (2007) [*Quantum Electron*., **37**, 1153 (2007)].
25. Fibich G., Gaeta A. *Opt. Lett.*, **25**, 335 (2000).
26. Kosareva O.G., Liu W., Panov N.A., Bernhardt J., Ji Z., Sharifi M., Li R., Xu Z., Liu J., Wang Z., Ju J., Lu X., Jiang Y., Leng Y., Liang X., Kandidov V.P., Chin S.L. *Laser Phys.*, **19**, 1776 (2009).
27. Daigle J.-F., Kosareva O.G., Panov N.A., Begin M., Lessard F., Marceau C., Kamali Y., Roy G., Kandidov V.P., Chin S.L. *Appl. Phys. B*, **94**, 249 (2009).